Remote Sensing of Environment 112 (2008) 3563–3581

Contents lists available at ScienceDirect

Remote Sensing of Environment

journal homepage: www.elsevier.com/locate/rse

Snow optical properties for different particle shapes with application to snow grain size retrieval and MODIS/CERES radiance comparison over Antarctica

Zhonghai Jin [a,*], Thomas P. Charlock [b], Ping Yang [c], Yu Xie [c], Walter Miller [d]

[a] Science Systems and Applications, Inc., One Enterprise PKWY, STE 200, Hampton, VA 23666, United States
[b] Mail Stop 420, Climate Science Branch, Science Directorate, NASA Langley Research Center, Hampton, Virginia 23681-2199, United States
[c] Department of Atmospheric Sciences, Texas A&M University, College Station, TX 77843, United States
[d] Science Systems and Applications, Inc., One Enterprise PKWY, STE 200, Hampton, VA 23666, United States

ARTICLE INFO

Article history:
Received 7 January 2008
Received in revised form 18 April 2008
Accepted 19 April 2008

Keywords:
Snow
Radiative transfer
Radiance
Snow grain size retrieval

ABSTRACT

We investigated the single scattering optical properties of snow for different ice particle shapes and degrees of microscopic scale roughness. These optical properties were implemented and tested in a coupled atmosphere-snow radiative transfer model. The modeled surface spectral albedo and radiance distribution were compared with surface measurements. The results show that the reflected radiance and irradiance over snow are sensitive to the snow grain size and its vertical profile. When inhomogeneity of the particle size distribution in the vertical is taken into account, the measured spectral albedo can be matched, regardless of the particle shapes. But this is not true for the modeled radiance distribution, which depends a lot on the particle shape. The usual "equivalent spheres" assumption significantly overestimates forward reflected radiances, and underestimates backscattering radiances, around the principal plane. On average, the aggregate shape assumption has the best agreement with the measured radiances to a mean bias within 2%. The snow optical properties with the aggregate assumption were applied to the retrieval of snow grain size over the Antarctic plateau. The retrieved grain sizes of the top layer showed similar and large seasonal variation in all years, but only small year to year variation. Using the retrieved snow grain sizes, the modeled spectral and broadband radiances showed good agreements with MODIS and CERES measurements over the Antarctic plateau. Except for the MODIS 2.13 μm channel, the mean relative model-observation differences are within few percent. The modeled MODIS radiances using measured surface reflectance at Dome C also showed good agreement in visible channels, where radiation is not sensitive to snow grain size and the measured surface bidirectional reflectance is applicable over the Antarctic plateau. But modeled radiances using local, surface-measured reflectance in the near infrared yielded large errors because of the high sensitivity to the snow grain size, which varies spatially and temporally. The CERES broadband shortwave radiance is moderately sensitive to the snow grain size, comparable to the MODIS 0.86 μm channel. The variation of broadband snow reflectance due to the seasonal variation in snow grain size is about 5% in a year over the Antarctic plateau. CERES broadband radiances simulated with grain sizes retrieved using MODIS are about 2% larger than those observed.

1. Introduction

Snow is the most reflective surface type on Earth, and it plays an important role in the surface energy budget of polar regions and climate of the globe. The albedo of snow has a pronounced spectral variation, from almost unity in the visible to almost zero in the near infrared. Because of the complexity of particle shape, the accurate calculation of the single scattering properties of a snow grain is a challenge. "Equivalent spheres" with same volume-to-surface ratio as the actual snow grains are commonly used to represent snow grains (ice crystals) in radiative transfer models (e.g., Wiscombe and Warren, 1980; Nolin and Dozier, 2000; Li and Zhou, 2004; Painter and Dozier, 2004), even though actual snow particles are quite non-spherical. The "equivalent sphere" parameterization allows the use of Mie theory for computation of single scattering parameters. This simplified approach can successfully simulate hemispherically averaged radiative quantities, such as irradiance and albedo (Grenfell et al., 1994; Aoki et al., 2000), which are not very sensitive to the finer aspects of the scattering phase function. The scattering phase function for an ice crystal is closely related to particle shape; the phase function of non-spherical particles may differ dramatically from those of spheres, and yet have the same asymmetry factor. Directional quantities, such as bidirectional reflectance and radiance, are however more sensitive to scattering phase function and hence to particle shape (Mishchenko et al., 1999; Kokhanovsky and Zege, 2004; Xie et al., 2006). A sound

* Corresponding author.
E-mail address: Zhonghai.Jin@nasa.gov (Z. Jin).

0034-4257/$ – see front matter © 2008 Elsevier Inc. All rights reserved.
doi:10.1016/j.rse.2008.04.011

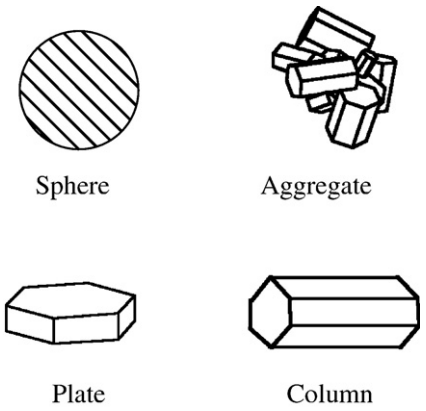

Fig. 1. The four idealized shapes of the snow particle habits.

theoretical model of radiance that accounts for the effects of particle shape is a vital tool for advancing the retrieval of snow characteristics (i.e., snow grain size, surface irradiance) with satellite radiances.

The Antarctic plateau is covered by dry, clean, cold snow all year; the plateau has few aerosols and little water vapor. Satellite measured radiances in the solar spectrum over the Antarctic plateau are dominated by the effects of snow. Therefore, the Antarctic plateau is an ideal location to test the theory of snow optical properties, radiative transfer in snow and snow property retrieval algorithms.

NASA's Earth Observation System satellites, which view the Antarctic plateau several times per day, now have a multi-year record. In particular, the Moderate-resolution Imaging Spectroradiometer (MODIS) sensors on Terra and Aqua measure narrow-band radiances in various shortwave (SW or solar) bands, while Clouds and the Earth's Radiant Energy System (CERES) sensors on the same satellites measure broadband SW radiances simultaneously (Wielicki et al., 1996). These coincident narrow-band and broadband measurements provide an excellent database for studies of snow with radiative transfer models. Using CERES-retrieved clouds using MODIS imager (Minnis et al., 2003) and MODIS-retrieved aerosols (Kaufman et al., 1997), and a data assimilation of temperature and humidity (GEOS4 described by Bloom et al., 2005), CERES also computes the Surface and Atmospheric Radiation Budget (SARB, Charlock et al., 2006) at five levels. Comparisons of calculated and observed SW fluxes at both the top of atmosphere (TOA) and the ground are less favorable at high latitudes, in part because of the parameterization of snow. While the fluxes calculated for a cloudy sky, for example, benefited by using inputs like cloud particle size retrieved from MODIS data, explicit retrievals of snow particle size were simply not available.

In this paper, we present the snow optical properties based on different assumptions of ice crystal shape and roughness, compare them with those from Mie theory, and implement them in a coupled atmosphere-snow radiative transfer model. The simulations are compared to quality surface and satellite measurements and then

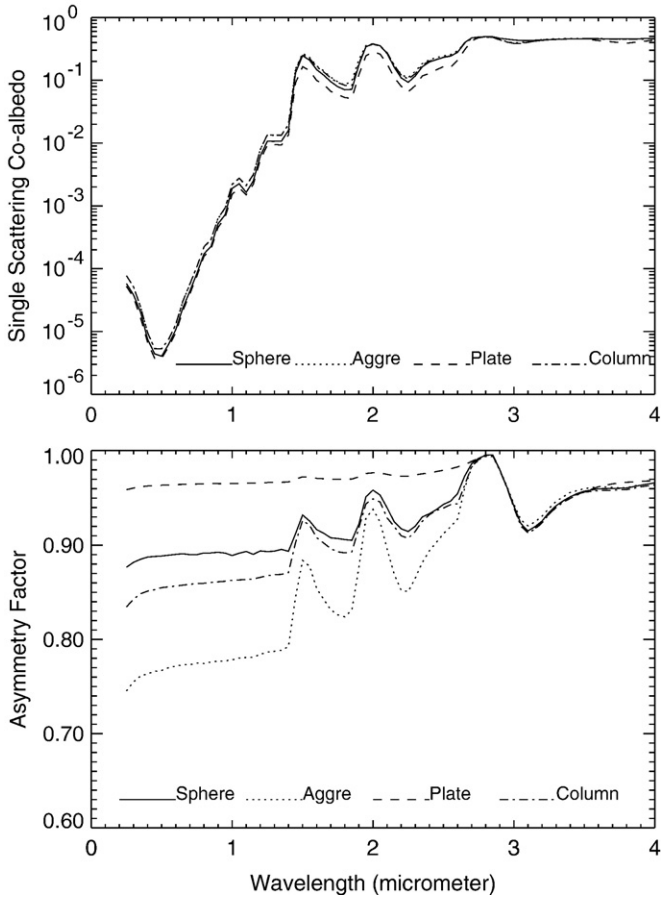

Fig. 3. The single scattering co-albedo (the upper panel) and asymmetry factor (the lower panel) as a function of wavelength for the four particle shapes. RE = 100 μm.

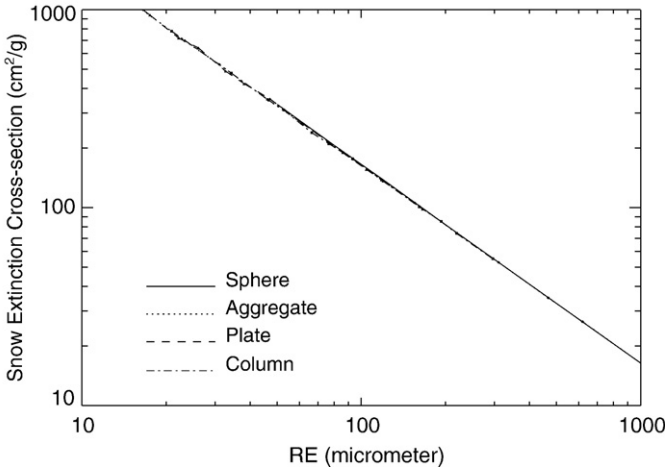

Fig. 2. Comparison of the total extinction cross-section in 1 g of snow as a function of particle effective radius (RE) for the four particle shapes shown in Fig. 1. λ = 0.55 μm.

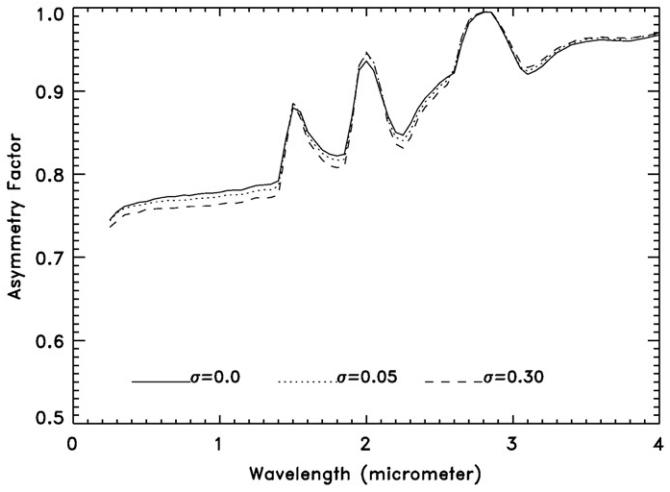

Fig. 4. Effect of ice particle (aggregate) surface roughness (σ) on the asymmetry factor. RE = 100 μm.

applied to retrieve the sizes of the snow grains. The objective of this paper is to demonstrate various effects of snow properties on the radiation over snow in different parts of the shortwave spectrum; to find an appropriate particle shape for simulating observed radiances; to find the viewing geometries that are useful for snow property retrievals; and to test a model of snow for future applications with SW satellite data.

2. Single scattering optical properties of snow

The extinction coefficient, single scattering albedo (SSA), and scattering phase function are fundamental in radiative transfer models. For many computations, especially for angular average quantities such as irradiance and albedo, a simple Henyey–Greenstein phase function (HG) is employed; commonly the HG with the same asymmetry factor as the actual phase function (Henyey and Greenstein, 1941). Only the asymmetry factor is needed to define HG.

The single scattering optical properties of snow vary intricately with grain size, particle shape, microscopic crystal surface roughness and wavelength. The optical properties in this study are based on four idealized particle shapes: spheres, aggregates of columns, hexagonal plates and solid hexagonal columns, as illustrated in Fig. 1. The optical properties for spheres are based on Mie theory, while those for non-spherical particles are computed from an improved geometric-optics method (IGOM) developed by Yang and Liou (1996). The refractive index for these computations is from Warren (1984). Fig. 2 compares the extinction cross-section of unit mass (1 g) of snow at 0.55 μm for the four particle shapes shown in Fig. 1. The *x*-axis in Fig. 2 represents the effective radius (RE) of the ice particle (snow grain size). RE is defined as

$$\mathrm{RE} = \frac{3}{4}(V/A) \tag{1}$$

where V and A represent the particle volume and projected area respectively. For spheres, the RE is the same as the actual radius. Fig. 2 includes grain sizes from 10 μm (smaller than typically found in fallen snow) to 100 μm (roughly characteristic of the Antarctic plateau during summer, but also found elsewhere atop fresh, cold snow fields) and 1000 μm (typical grain size for aged melting snow). The extinction per unit mass is very similar throughout the SW spectrum, because the sizes of these grains are much larger than the optical wavelengths. Fig. 2 shows that the extinction of snow varies greatly with snow grain size, but varies little with particle shape, for a same mass of snow.

Fig. 3 compares the single scattering co-albedo (upper panel) and asymmetry factor (lower panel) for the same four particle shapes as Fig. 2. Fig. 3 shows that while the effect of particle shape on co-albedo is modest but significant, shape has a more substantial effect on asymmetry factor (g). The g for plates is larger than that for spheres, because a number of rays transmit through two parallel basal faces without changing their propagating direction in the case of plates, contributing to the increase of g. And unlike the extinction coefficient, both co-albedo and asymmetry factor vary strongly with wavelength for all shapes.

We now consider microscopic scale roughness of the particle surface. Micro-roughness affects the optical properties of individual snow grains. In the computation, the normal of the particle surface is statistically perturbed for each reflection–refraction event. The distribution of the normals or slopes (s) of the facets of a roughened surface is described by the Gram–Charlier function (Cox–Munk, 1954) as

$$p(s) = \frac{1}{\pi\sigma^2}\exp\left(-\frac{s^2}{\sigma^2}\right) \tag{2}$$

where σ is the mean slope distribution width. Large σ indicates a rough surface, and zero σ indicates a completely flat surface. The technical details of the treatment of surface roughness are reported in Yang and Liou (1998). This surface micro-roughness has almost no effect on the total extinction and absorption, but it has some effect on the scattering phase function. Increasing the surface roughness reduces the forward scattering peak and tends to smooth the entire phase function. Fig. 4 shows the asymmetry factors of three different roughness parameters (σ) for particles of aggregate shape with RE = 100 μm.

The asymmetry factor is much more sensitive to particle shape (Fig. 3, lower panel) than to particle micro-roughness (Fig. 4), for the regimes considered here.

Because of the strong influence of shape on the optical properties of an individual snow particle, the shape assumed by a model affects the radiances calculated for the entire snow field. The upper panel of Fig. 5 shows the effect of particle shape on simulated snow surface albedo for a diffuse incidence with RE of 100 μm. For the same effective size RE, aggregates have the highest albedo, whereas plates have the lowest. Spheres and solid columns produce similar surface spectral albedos (Fig. 5), because they have similar asymmetry factors (Fig. 3); however their scattering phase functions (which influence directional reflectance) are very different. The lower panel of Fig. 5 (also for RE of 100 μm) shows the small effect of particle micro-roughness on the surface albedo of the snow field; roughness has small influence on the asymmetry factor (and albedo) but more on the scattering phase function (and directional reflectance).

3. Comparison with surface measurements

To test the theoretical single scattering optical properties of snow particles, we implemented them in a coupled atmosphere-snow radiative transfer model and compared model results with measurements over a snow field. The model is coupled: it treats scattering and

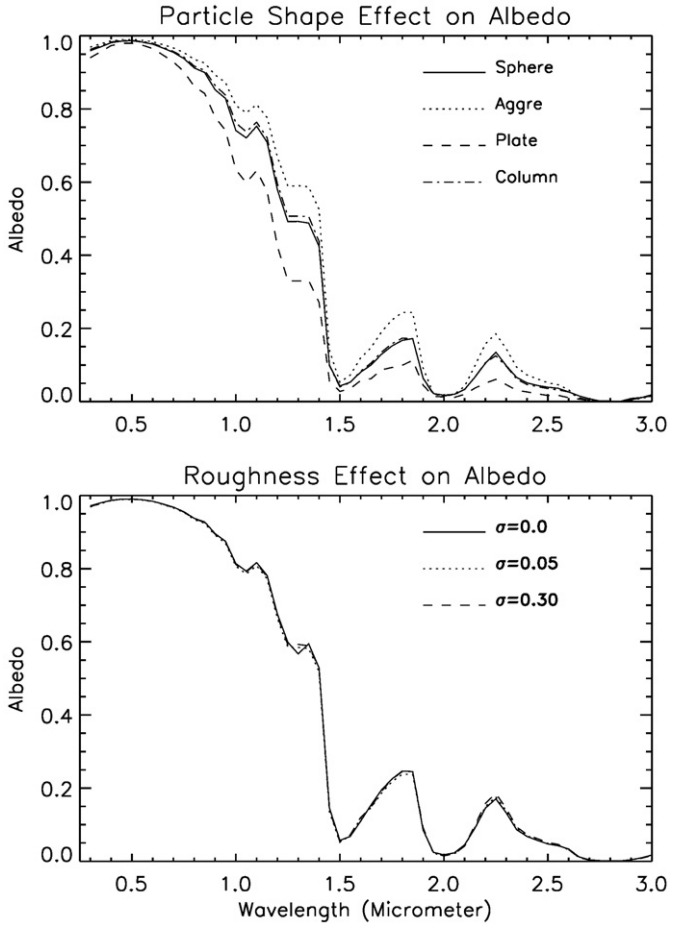

Fig. 5. Effects of snow particle shape (the upper panel) and surface roughness (the lower panel) on the calculated snow surface albedo. RE = 100 μm.

absorption within both media (atmosphere and snow) explicitly, rather than using one medium as a simple boundary condition for the other. Except for the idealized shapes of individual snow grains, the model is plane parallel. The snow grains are oriented randomly. We do not account for macroscale variations of the snow field (i.e., sastrugi or snow drifts). The radiative transfer model can calculate the spectral and broadband radiances and irradiances at any level of the atmosphere and snow. Similar to the atmosphere, the snow can also be divided into an arbitrary number of layers to resolve, for example, the variation of snow grain size with depth. Optionally, the snow surface can also be considered as the bottom boundary, when the coupled model becomes a conventional atmospheric radiative transfer model and the snow surface reflectance is required as input. More description on the radiative transfer model was presented in Jin et al. (2006).

The measurements were made at Dome C (75.1°S, 123.3°E) on the Antarctic plateau by Hudson et al. (2006). They measured both the spectral albedo of the snow surface and the angular variation of radiances from a 32 m tower over a thorough range of viewing geometry. The measurement domain included the effects of sastrugi (when present) but not very large scale effects like mountains.

Fig. 6 compares the modeled and measured diffuse spectral albedo of snow. Each of the four panels corresponds to the respective particle shape assumed by the model. The measurements, represented by plus signs, are identical in all panels. Dashed lines give the model results assuming both single-layer snow (which does not change with depth) and the smallest RE of the respective panel; these match the measurements in all panels quite well in longer wavelengths (>1400 nm) but overestimate the albedo in shorter wavelengths. Dotted lines have model results also assuming single-layer snow, but with the largest RE of the respective panel; the large RE results match the measurements in shorter wavelengths but instead underestimate the albedo in longer wavelengths. The solid lines are results from a two-layer snow model in which the top layer (h=0.5 mm) has the smaller RE, and the bottom layer has the larger RE, of the respective panels. The optical depth for the bottom layer can be considered to be infinite because of the snow thickness over Antarctic plateau. Fig. 6 shows that if a two-layer snow model is used, or if the snow grain size and its vertical profile are both freely adjustable parameters, the observed spectral albedo can then be suitably matched with any of the four assumptions for particle shape. However, the effective radii (RE) required to match the spectral albedos differ among the particle shapes, because the single scattering optical properties for RE (as defined by Eq. (1)) depend on particle shape. Grenfell et al. (1994) also matched the spectral albedo measured at the South Pole by using two-layer snow (RE=30/100 μm) with the spherical particle assumption.

Using the same two-layer snow models that matched the spectral albedo shown in Fig. 6, we calculated the angular distribution of radiances for comparison with the measured Anisotropic Reflectance Factor (ARF). ARF is defined as

$$\mathrm{ARF}(\theta,\phi)=\frac{\pi I(\theta,\phi)}{E_0}=\frac{r(\theta,\phi)}{\alpha} \tag{3}$$

for view zenith angle θ and, relative azimuth angle ϕ, reflected radiance $I(\theta,\phi)$, and reflected irradiance E_0. It equals to the ratio of the reflectance $r(\theta,\phi)$ and the albedo (α). Note that ARF corresponds to a

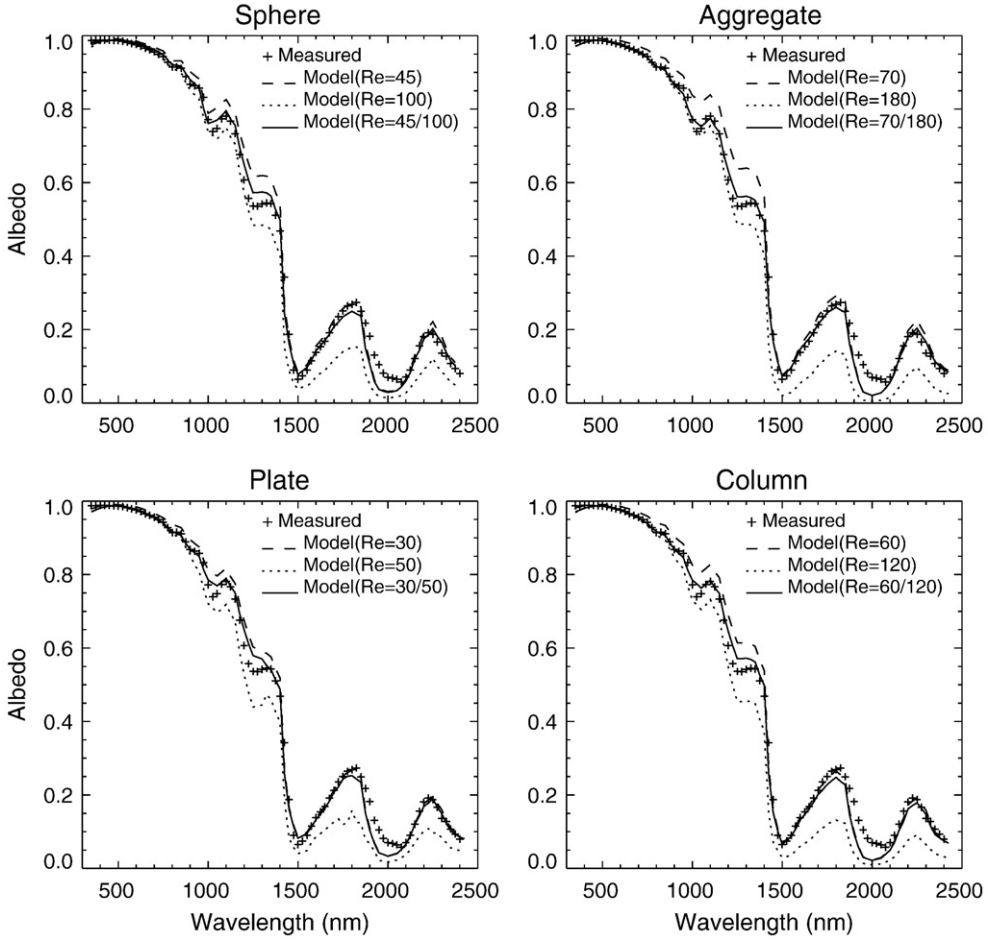

Fig. 6. Comparison of modeled and measured snow surface albedo at Dome C, Antarctic. The four panels are for the four particle shapes respectively. In each panel, the dashed and dotted lines are modeled albedo using a single-layer snow model, whereas the solid line shows the model results using a two-layer snow model. All measurements are ground-based.

particular solar zenith angle (θ_o). The hemispheric average of ARF is unity. Both ARF and the bidirectional reflectance distribution function (BRDF) are used to describe the angular distribution of reflected radiances. A complete BRDF observation would measure (sample) all the reflected (upwelling) radiances for each of a full incident (downwelling) radiance distribution. BRDF at some wavelengths can be quite difficult to observe in the field, because surfaces are typically illuminated by incoming diffuse skylight at many angles simultaneously. As such scattered downwelling radiation in the near infrared (NIR) is minimal during clear conditions over the Antarctic plateau, the NIR ARF and downwelling NIR flux at a given solar elevation and azimuth then effectively constitute the NIR BRDF for that solar elevation and azimuth.

Fig. 7 is an example of the simulated ARF compared with tower measurements for a solar zenith angle (θ_o) of 60.27° at wavelength 650 nm, near the center of MODIS channel 1. The same two-layer snow

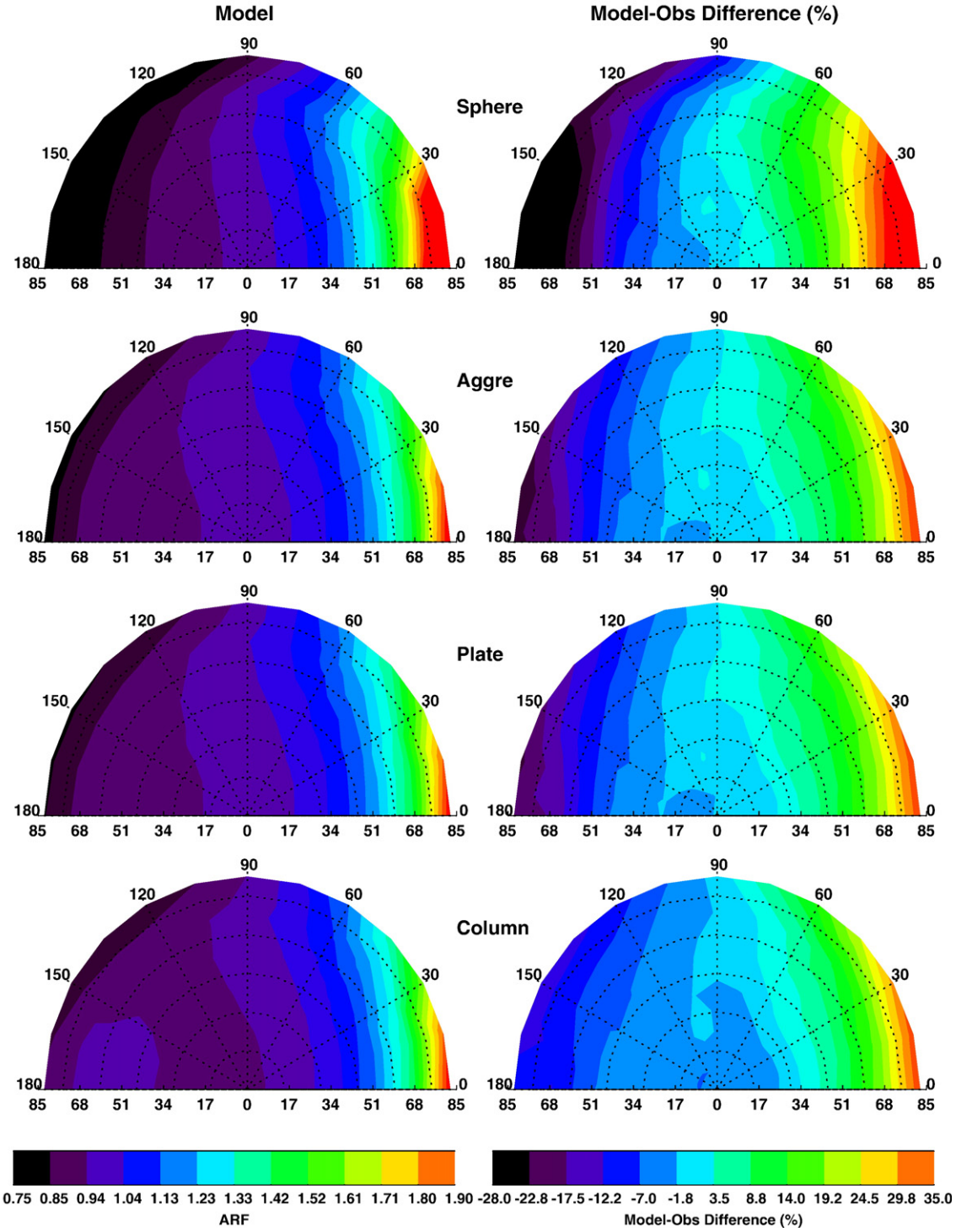

Fig. 7. Comparison of modeled and measured radiance distribution (ARF) at solar zenith angle (θ_o) 60.27° over snow surface at Dome C, Antarctic. The left panels show model results. The right panels show the model discrepancy with measurement in percent [100×(model-measurement)/(measurement)]. The four rows are for the four particle shapes respectively. Wavelength λ=0.65 μm. All measurements are ground-based.

models as used in the solid lines of Fig. 6 (for matching the spectral albedo) are used here. The left panels of Fig. 7 show the modeled ARF, and the right panels show the relative model-observation difference in percentage; each row has one particle shape; view zenith angle is the horizontal coordinate; relative azimuth angle is marked on the semi-circle. The ARF is assumed to be symmetric with the principal plane (the vertical plane containing the sun, the surface target and the nadir), so only azimuths from 0° to 180° are presented. The entire principal plane is covered by the horizontal axis of each panel, and the sun is on the left. Generally, the ARF or reflectance for forward scattering (azimuth angle<90°) at large zenith view angle is overestimated by the model, but it is underestimated for backward scattering (azimuth>90°) at large view zenith angle, especially for calculations using spherical particles (upper row in Fig. 7). However, for simulations using non-spherical particles (the lower three rows) the relative discrepancies with measurements are mostly less than 10% for view zenith angles less than 60°. Note that most satellite observations are from view zenith angle less than 60°. Large ice crystals have strong forward scattering, but they also have a secondary reflection peak directly backward. The theoretical scattering phase function has larger errors there, although we removed the diffraction and transmission peaks in the calculations. This contributes to large discrepancies between simulated and observed radiances at large view zenith angles close to the principal plane, as shown in Fig. 7. Another cause of this error is the macroscopic snow surface roughness, which decreases forward reflection (i.e., shadow cast by sastrugi) and enhances backward reflection, when compared with the flat surface used in the model (Warren et al., 1998).

Model simulations for other wavelengths and solar zenith angles also compare favorably with ground observations. Fig. 8 shows the discrepancies of the model mean ARF with respect to ground observations as fractions (i.e., a discrepancy of 0.02 in Fig. 8 is equivalent to 2% in Fig. 7) for two MODIS channels and solar zenith angle (θ_o) 60.27°. The asterisk is for all view angles measured and the square is for view angles less than 60°. The discrepancies of model ARF for the two channels are similar.

The upper right panel of Fig. 7 shows that calculations using the spherical particle assumption significantly overestimate forward reflection, and underestimate backward reflection, near the principal plane. The spherical assumption is not a good choice for computing directional reflectance over snow. Among the three non-spherical particle assumptions, the aggregate presents the best agreement with measurements on average. Based on the results shown above and others not shown, we assume aggregate snow particles for subsequent radiative transfer computations. The particle surface roughness parameter (σ) used in Figs. 6–8 is 0.30, as for the dashed line in Fig. 4. On average, this microscopic roughness has little effect; simulations using σ of 0.30 have a slightly better match with measurements than do simulations using a smaller σ (less roughness). There is yet no measurement of σ for snow. Larger σ gives a smoother scattering phase function. The variation of particle size in an actual snowpack also tends to smooth the collective scattering phase function.

4. Snow grain size retrieval

We now consider the retrieval of snow grain size with MODIS data. In situ observations over the Antarctic plateau indicate that grain size often changes sharply with depth, the typical thin top layer consisting of small, fresh snow grains (Grenfell et al., 1994; Gay et al., 2002). Fig. 6 shows the sensitivity of the spectral albedo of snow to grain size and its vertical profile. While reflection to TOA in the near infrared is conveniently quite sensitive to the grain size, near infrared radiation is absorbed very quickly in the top layer of snow. This argues for including a second MODIS channel in the visible when retrieving grain sizes. With less sensitivity to grain size, but more ability to penetrate, the visible channel can provide some information on the bottom layer.

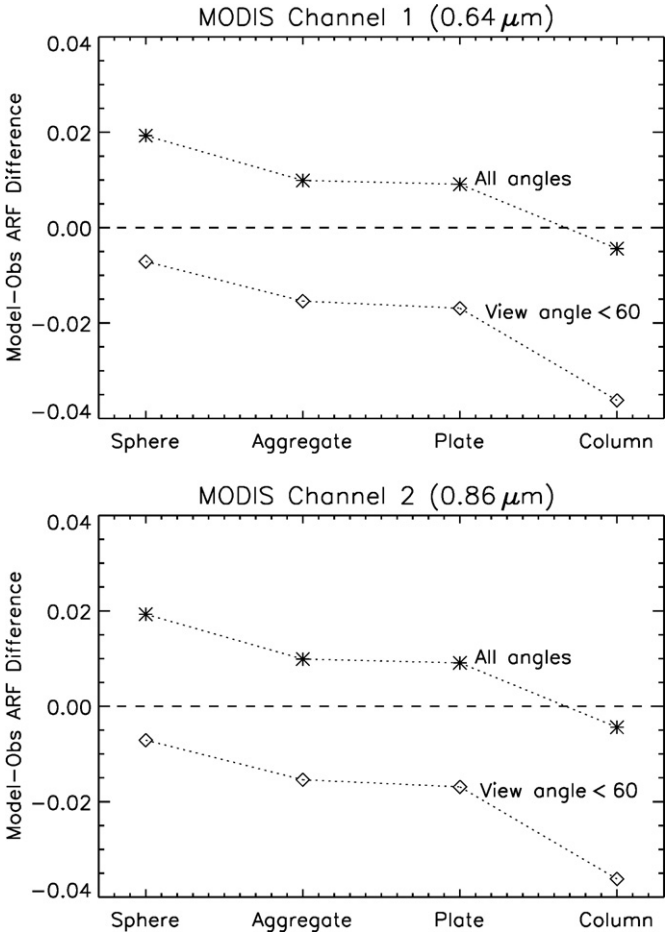

Fig. 8. The mean ARF model discrepancy with measurement as a fraction [(model-measurement)/(measurement)] for MODIS channel 1 (the upper panel) and channel 2 (the lower panel) at solar zenith angle (θ_o) 60.27°. The asterisk denotes that the mean ARF is obtained from an integration over all view zenith angles measured. The square denotes mean ARF from an integration over only view zenith angles less than 60°. All measurements are ground-based.

We adopt a two-layer snow model with aggregate shape (as in the solid line in the upper right panel of Fig. 6) and choose MODIS channel 6 (1.64 μm) for the top layer snow grain size retrieval and channel 1 (0.64 μm) for the bottom layer size retrieval. Two reflectance look up tables (LUT) corresponding to the two MODIS channels were developed. As in Fig. 6, the top layer has a geometrical thickness of 0.5 mm. Grain size is assumed to be constant within each layer. The sub-arctic winter (SAW) atmospheric model of McClatchey et al. (1972) was used for the tables. The vertical profile of water vapor is fixed, but the total precipitable water varies with the surface elevation. The total water vapor amount is small over the Antarctic plateau (Chamberlin, 2001), and its absorption in both MODIS channels is very small. In each table, the reflectance at the top of atmosphere (TOA) is a function of solar zenith angle, satellite view zenith angle, relative azimuth angle, elevation of surface above sea level, and aerosol optical thickness (AOT); as AOT over the Antarctic is generally low, it is set as zero in this study. In addition to these five parameters, the reflectance table for the 0.64 μm channel has two additional dependent variables: total ozone amount and grain size of the top layer. The algorithm first matches the MODIS 1.64 μm reflectance with the LUT to obtain the snow grain size of the top layer. Then the top layer grain size and the other parameters are used to match the 0.64 μm reflectance, thus obtaining the grain size of the bottom layer. Also, the bottom layer grain size is required to be larger than or equal to the first layer size. If a value for the bottom layer grain

size returned by applying the LUT is less than the top layer size, it is reset to the size of the top layer.

The CERES and MODIS data used here are from NASA's Terra satellite. We retrieve the snow grain size for only the clear CERES footprints (~20–40 km). Clouds were screened by the CERES cloud algorithm (Minnis et al., 2003), which employs several channels of high spatial resolution MODIS imager (~1–2 km) data. The MODIS observed radiance are the energy weighted average of the pixels in

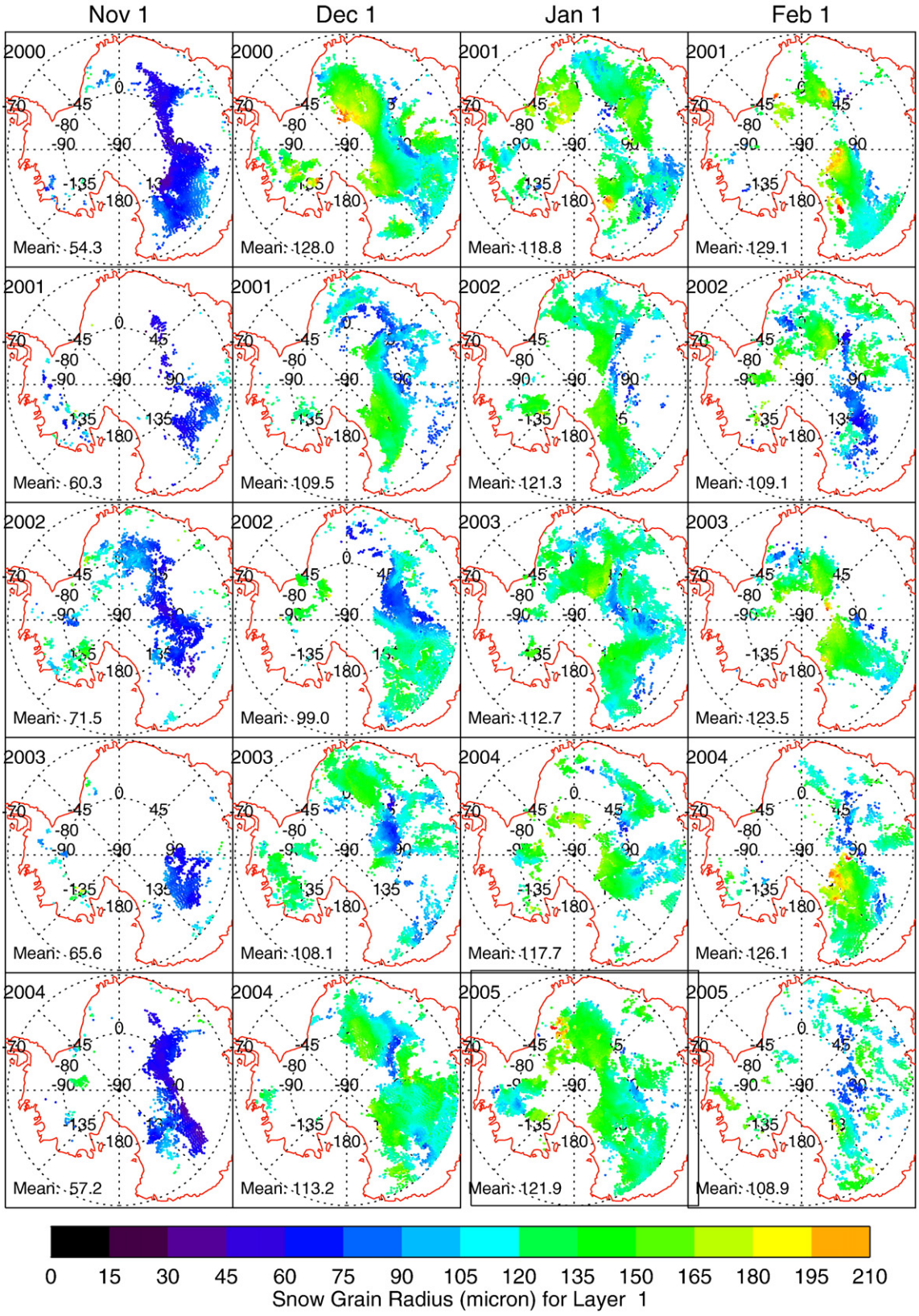

Fig. 9. Retrieved snow effective radius (RE) for the top layer of snow over the Antarctic plateau in the five summers from 2000 to 2005 (four days per year) using MODIS data.

each CERES footprint, using the CERES point spread function (PSF) (Priestley et al., 1997). In each clear CERES footprint, the PSF-weighted standard deviations of MODIS radiances for two channels are used to detect macroscale roughness of the snow surface. The relative standard deviation of the 0.64 μm (1.64 μm) MODIS radiances within a CERES footprint must be less than 0.02 or 2% (0.04 or 4%). This filters

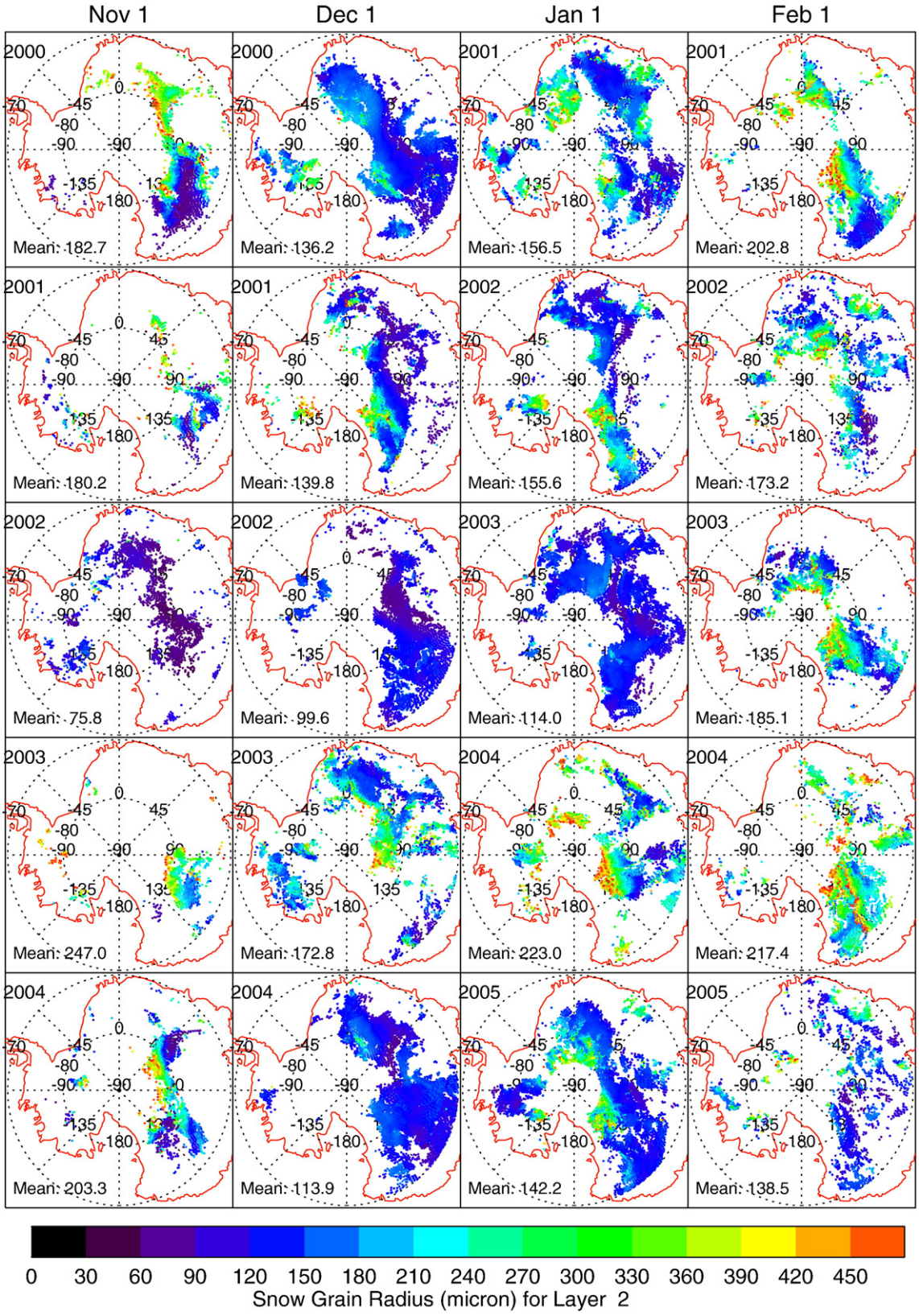

Fig. 10. Similar to Fig. 9, but for the bottom layer of snow.

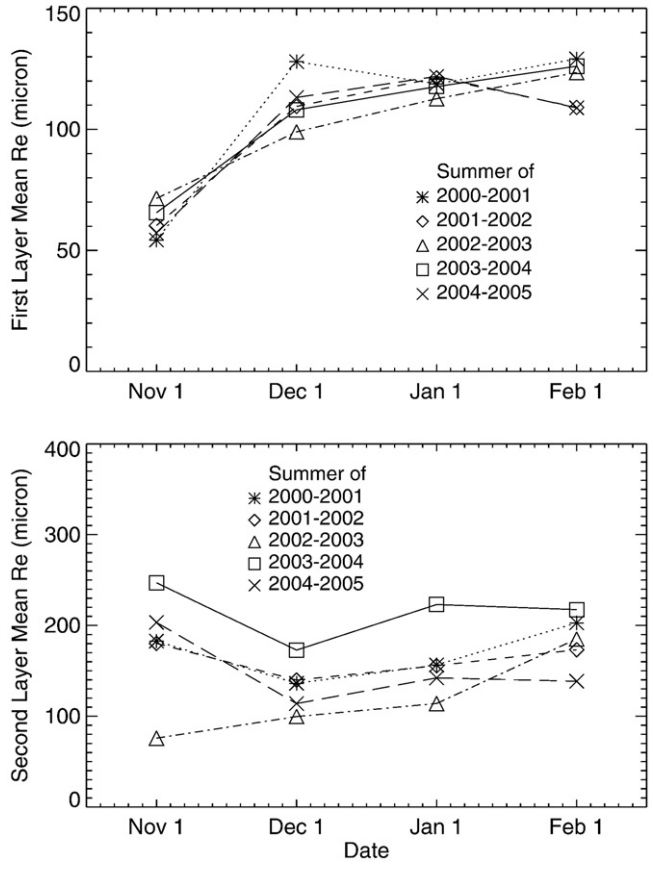

Fig. 11. The seasonal variation of the mean snow RE over the Antarctic plateau in the five summers shown in Fig. 9 and Fig. 10.

out footprints with large scale surface inhomogeneity, but not those with macroscale snow surface roughness that is more uniformly distributed.

Fig. 9 shows the retrieved top layer snow grain size (effective radius, RE) over the Antarctic plateau (latitude > 70°) for four days, each the first of a respective month, during five summers from 2000 to 2005. In each year, the snow grain size in early summer is the smallest. Year-to-year variations are less than seasonal variations. Based on a comparison of computed radiances with observations (Fig. 7 in Section 3), both retrievals of grain size at forward scattering angles with view zenith larger than 30°, and also those at backscattering angles with view zenith larger than 60°, have been excluded. Fig. 10 is similar to Fig. 9, but for the bottom layer snow grain size. Fig. 11 shows the average sizes retrieved over the Antarctic plateau for each summer (using the first-day-of-month domain as Figs. 9–10). The bottom layer snow grain size is larger than the top layer and it does not show the seasonal variation as those in the top layer, which increased from November to December. The vertical distribution of grain size in actual snow is not uniform. The sizes retrieved here should thus be regarded as roughly weighted averages. Our results are, however, generally consistent with in situ measurements reported in the literature (Gay et al., 2002; Grenfell et al., 1994).

5. Retrieval error analysis

We now present a brief, theoretical error analysis of the retrieval algorithm for snow grain size. The error analysis uses 5000 forward radiative transfer calculations of the TOA radiances in the 1.64 μm and 0.64 μm bands based on the 2-layer snow model described above for the snow grain size retrieval. The 5000 pairs of snow grain sizes for the two layers and the retrieval geometry (solar zenith, view zenith and azimuth angles) for model input are created randomly within the following domains. Based on the results in Figs. 9–11, the first layer snow grain size (R1) is limited between 40 to 200 μm, while the second layer snow grain size (R2) is limited between 40 and 500 μm. Because the snow grain size at a given location in the Antarctic has a minimum value at the surface, we require that R2 exceed R1 for each pair of sizes as in the retrieval algorithm. The solar zenith angle is randomly distributed from 50° to 85°; the view zenith angle is between 0° and 70°; and the azimuth angle is from 0° to 360°. The sub-arctic atmospheric model is used in the radiance calculations. We then apply the snow grain size retrieval algorithm described above to retrieve the snow grain sizes and compare results with the synthetic input data as a truth test. Fig. 12 compares the snow grain sizes in the first layer. The *x*-coordinate shows the input size used in the forward radiative transfer calculations. The *y*-coordinate in the left panels shows the retrieved size and that in the right panels shows the retrieval–input difference. The first row (panels a1 and a2) shows results retrieved by using the exact radiances (1.64 μm) calculated in the synthetic data; this indicates the noise and systematic error due to the algorithm itself. The second (third) row of Fig. 12 shows results using the input theoretical radiances shifted upward (downward) by +1% (−1%); this tests for the sensitivity of retrieved snow grain size to an error in MODIS calibration. The black marks in each panel of Fig. 12 span all view angles, while the results in red exclude both large view angles (>60°) and strongly forward scattering angles (a review of Fig. 7 should provide motivation for the restrictions). The view angle restrictions for red marks are the same as those of the actual MODIS-based Antarctic retrievals of Figs. 9 and 10. Fig. 12 shows that the retrieved R1 is generally larger than the input value in the synthetic data. This systematic error is due to the effect of the second layer. When retrieving R1, R2 is not known, and the vertical profile of snow grain size is hence not accounted. But in the forward radiative transfer calculations of radiance, the R2 is required to equal or exceed R1. The residual signal of this larger R2 is a slight upward discrepancy in the retrieved R1 in the top row of Fig. 12. The middle and bottom rows illustrate the effect of a possible error in MODIS calibration at 1.64 μm on the snow grain size retrieved for the top layer: the ±1% biases of the input radiance have negligible effect on the retrieval of R1.

Fig. 13 is similar to Fig. 12, but for the second layer snow grain size retrieval using the 0.64 μm band. When retrieving R2, the first layer size R1 is known and is hence one of the input parameters. The results for R2 in Fig. 13 (top row) show no apparent effect of the systematic error in the prior retrieval of R1 in Fig. 12 (top row). The middle and bottom rows of Fig. 13 preview the impact of possible errors in MODIS calibration on R2 in the second layer. But quite differently than was the case for the R1 retrieval, the ±1% radiance biases have much larger effect on R2 retrieval, because reflected radiance in the 0.64 μm band (Fig. 13) is less sensitive to grain size than in the 1.64 μm band (Fig. 12). Viewing geometry is yet another issue; black (red) marks use all (restricted) view angles. The marks in Figs. 12 and 13 show that theoretical errors in both R1 and R2 are reduced significantly if the view geometry is restricted, as in the actual Antarctic snow grain size retrieval of Section 4.

Table 1 summarizes the retrieval errors for grain sizes (R1 and R2) with respect to the input of synthetic data. The unit is in micrometer, but the numbers in parentheses are the relative bias in percent. Using the unbiased radiative transfer radiance (RT Rad in Table 1), the relative standard deviation discrepancy is 5.7% for R1 and 4.0% for R2.

We also determined the effect of retrieval errors in R1 and R2 on the TOA spectral reflectance. These calculations used the same atmospheric model and the 2-layer snow model as for the Antarctic snow grain size retrieval. Fig. 14 shows the nadir reflectance at TOA from 0.3 to 3.0 μm. The baseline calculations (the dotted lines in the upper two panels) assumed R1 = 100 μm and R2 = 180 μm (these values are approximate averages of the sizes retrieved over the Antarctic and shown in Fig. 11). The σ in Fig. 14 represents the grain size retrieval error presented by the standard deviation in Table 1. For example, $\sigma = 5.7\% \times R1 = 5.7$ μm for R1 (the left panels) and $\sigma = 4.0\% \times R2 = 7.2$ μm for R2 (the right panels). The solid and dashed lines in Panel (b1)

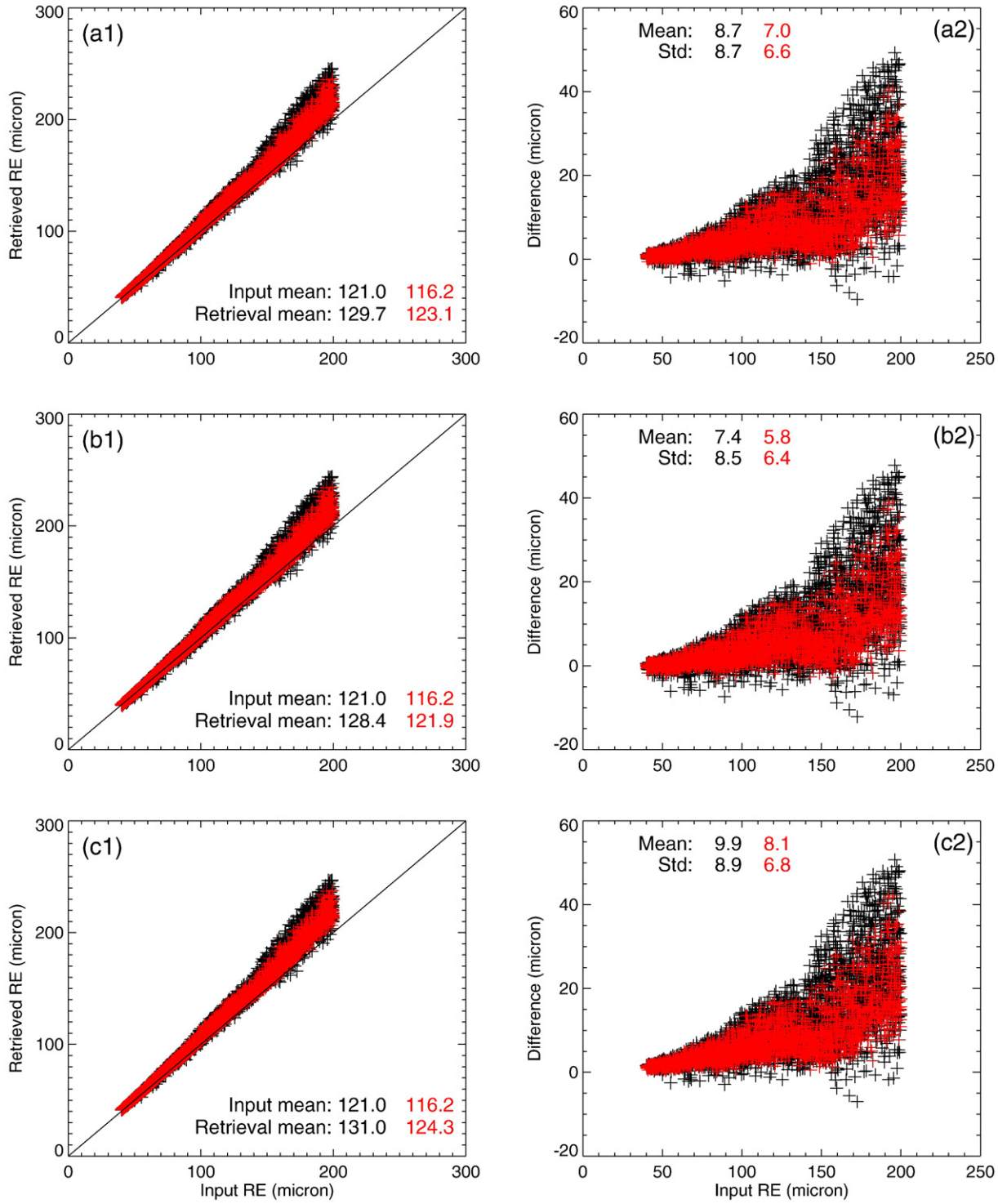

Fig. 12. Comparison of the retrieved first layer snow grain size with the input in the synthetic data. The retrieval in Panel (a1) is based on the unbiased radiances; that in Panel (b1) is based on the same radiances but with +1% bias; that in Panel (c1) has a −1% radiance bias. The black is for all angles and the red is for restricted angles. See text for details.

represent the reflectance biases due to the $+1\sigma$ and -1σ retrieval errors of R1 respectively (R2 = 180 μm), while the solid and dashed lines in Panel (b2) represent the reflectance biases due to the $+2\sigma$ and -2σ retrieval errors of R2 respectively (R1 = 100 μm). Fig. 14 shows that the effect of retrieval error in R1 on the TOA radiance is mainly in the near infrared, while the effect of error in R2 is mainly on wavelengths shorter than 1.4 μm.

The retrieval errors presented in this section are pertinent to the snow in the Antarctic, where snow grains are usually dry and small in size. For snow in other regions, where grains are often larger and wetter, and where the atmosphere has more effect on radiation, the retrieval algorithm here may not apply; more input data may be required.

6. Comparison with MODIS/CERES measured radiances

The spectral radiances measured by MODIS and the broadband radiances measured by CERES can be used to check both the single

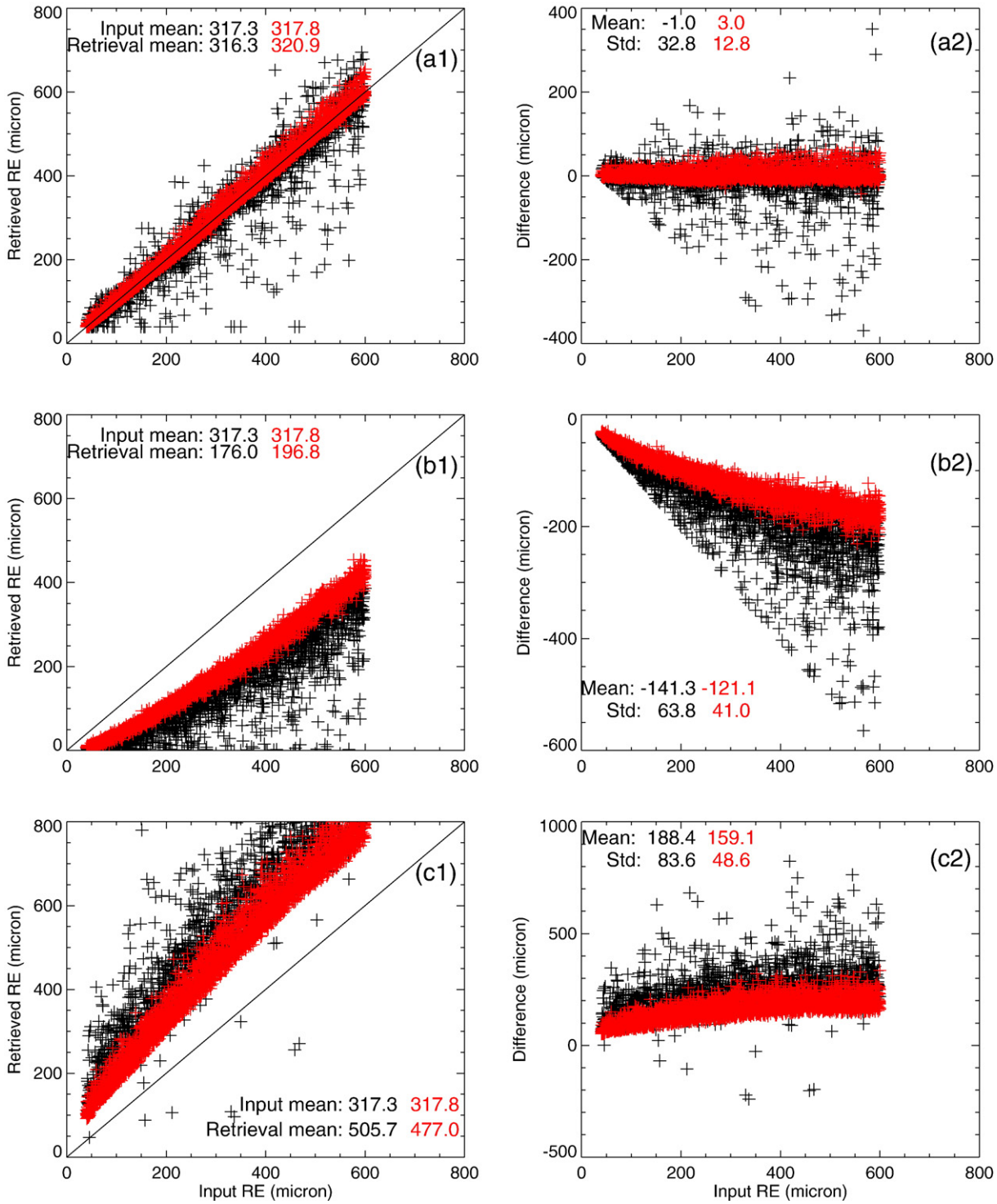

Fig. 13. Similar to Fig. 12, but for the second layer snow grain size.

scattering snow optical properties that we have assumed and the snow grain sizes that we have retrieved. We choose three representative MODIS channels for this test and compare simulated radiances with measurements. These three MODIS channels, which are independent of the two channels used for the grain size retrieval, also have different sensitivities to grain size (as does the CERES broadband SW). We use MODIS channel 4 (0.55 μm), channel 2 (0.86 μm) and channel 7 (2.13 μm). The 0.55 μm channel in the visible spectrum has small absorption in snow and is not sensitive to the snow grain size. In contrast, the 2.13 μm channel is very sensitive to the snow grain size, whereas the 0.86 μm channel is moderately sensitive to the gain size.

We calculated MODIS and CERES radiances for the clear CERES footprints with snow grain size retrievals shown in Figs. 9 and 10, but further restricted the domain to only those observations on the Antarctic plateau with surface elevation above 2500 m; this minimizes atmospheric effects and allows a focus on snow effects. As for all grain size retrievals, the standard deviations of MODIS radiances in each CERES footprint are used to screen out footprints with excessive surface roughness or with unidentified cloud

Table 1
The differences of snow grain size between the retrieved and the input in synthetic data

Layer	Mean difference			Std difference		
	RT Rad	+1% Rad	−1% Rad	RT Rad	+1% Rad	−1% Rad
1	7.0(6.0)	5.8(5.0)	8.1(7.0)	6.6(5.7)	6.4(5.5)	6.8(5.9)
2	3.0(0.9)	−121(− 38)	159.1(50.1)	12.8(4.0)	41.0(12.9)	48.6(15.3)

* Numbers in parentheses indicate relative difference in percent.

contamination. The grain sizes retrieved (based on LUTs for MODIS at 0.64 μm and 1.64 μm) are then used for the calculation of snow optical properties with the coupled atmosphere-snow model in radiance simulations for all wavelengths.

Fig. 15 compares the MODIS 0.55 μm channel radiances for the first days of the four summer months (four columns). For simplicity, each panel combines all five years of first days for the respective month (column). The upper two rows use the retrieved snow grain size for model input, whereas the lower two rows uses the measured surface reflectance (ARF) at Dome C (Hudson et al., 2006) for model input. Each MODIS observed radiance in Fig. 15 is the energy weighted average of those in each CERES footprint. Humidity (GEOS4) and ozone (National Centers for Environmental Prediction (NCEP) Stratosphere Monitoring Ozone Blended Analysis (SMOBA)) inputs for the radiative transfer calculations were obtained from the CERES database. The two sets of model calculations share the same atmospheric inputs but have different treatments of snow. The first set of radiative transfer calculations (the upper two rows in Fig. 15) is coupled and considers the two snow layers the same as atmospheric layers, whereas the second set of calculations (the lower two panels) is uncoupled and considers the snow surface as a bottom boundary for which the surface reflectance must be specified. When snow surface is treated as the bottom boundary in an uncoupled radiative transfer calculation, the snow physical and single scattering optical properties are not explicit inputs; the surface BRDF or the directional reflectance that represents snow is input. In our case, the available Hudson et al. (2006) measurement is a hemispherical–directional reflectance, which is different from the BRDF. The radiative transfer model was modified accordingly to input the ARF or the measured hemispherical reflectance. Fig. 15 demonstrates that the two independent approaches give similar results in this 0.55 μm channel. Although the ARF was measured at only one location, the uncoupled simulation using ARF (lower two rows) agrees with satellite data over much of the Antarctic plateau, almost as well as does the coupled simulation using retrieved sizes (upper two rows).

Similar to Fig. 15 (0.55 μm), Fig. 16 (0.86 μm) compares the two independent modeling approaches with MODIS observations. For both wavelengths, the standard deviations of discrepancies (simulation versus MODIS) using retrieved sizes (upper rows) are only a few

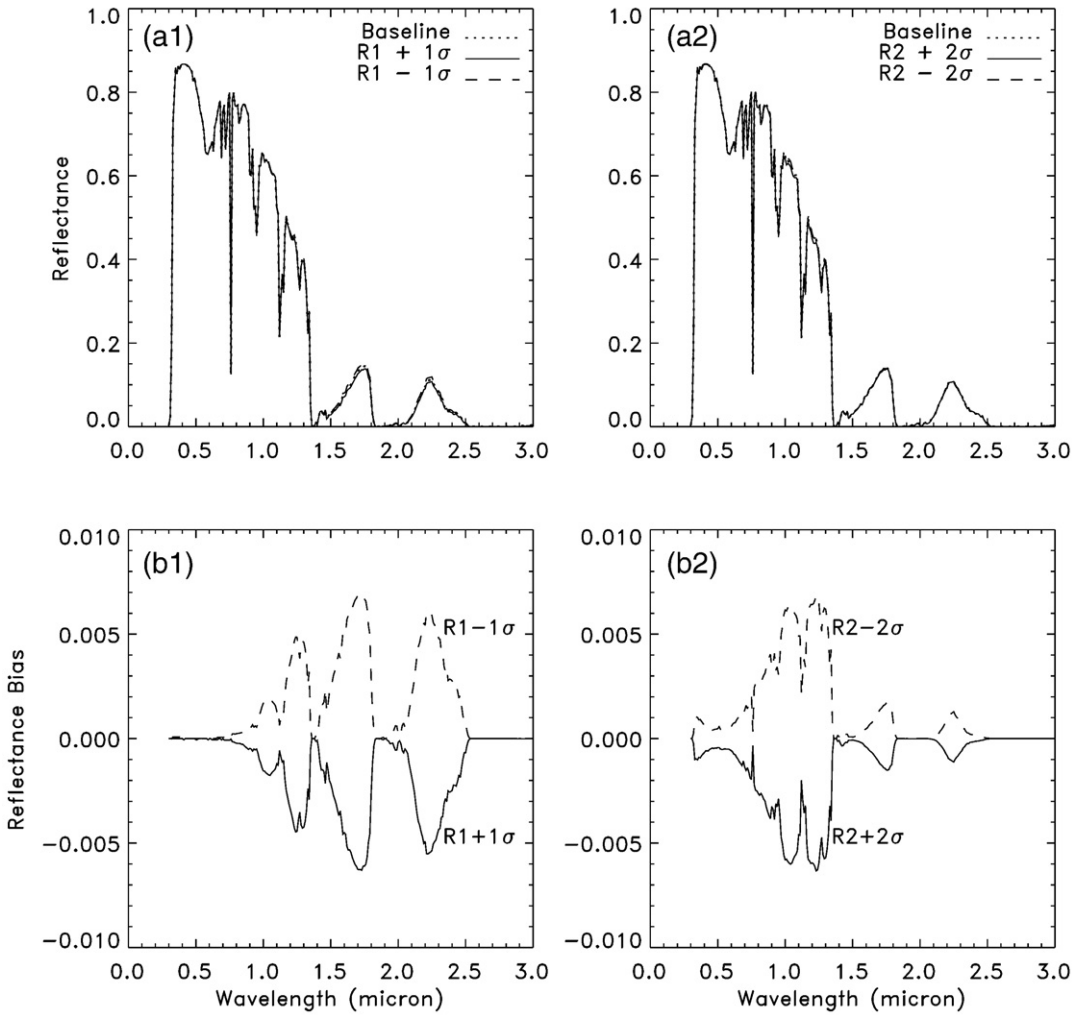

Fig. 14. The effect of the ±1σ retrieval errors in R1 (the left panels) and the ±2σ retrieval errors in R2 (the right panels) on the spectral TOA reflectance (nadir). R1 = 100 μm and R2 = 180 μm are used in the baseline calculations. The differences (Panels b1 and b2) are relative to the baseline.

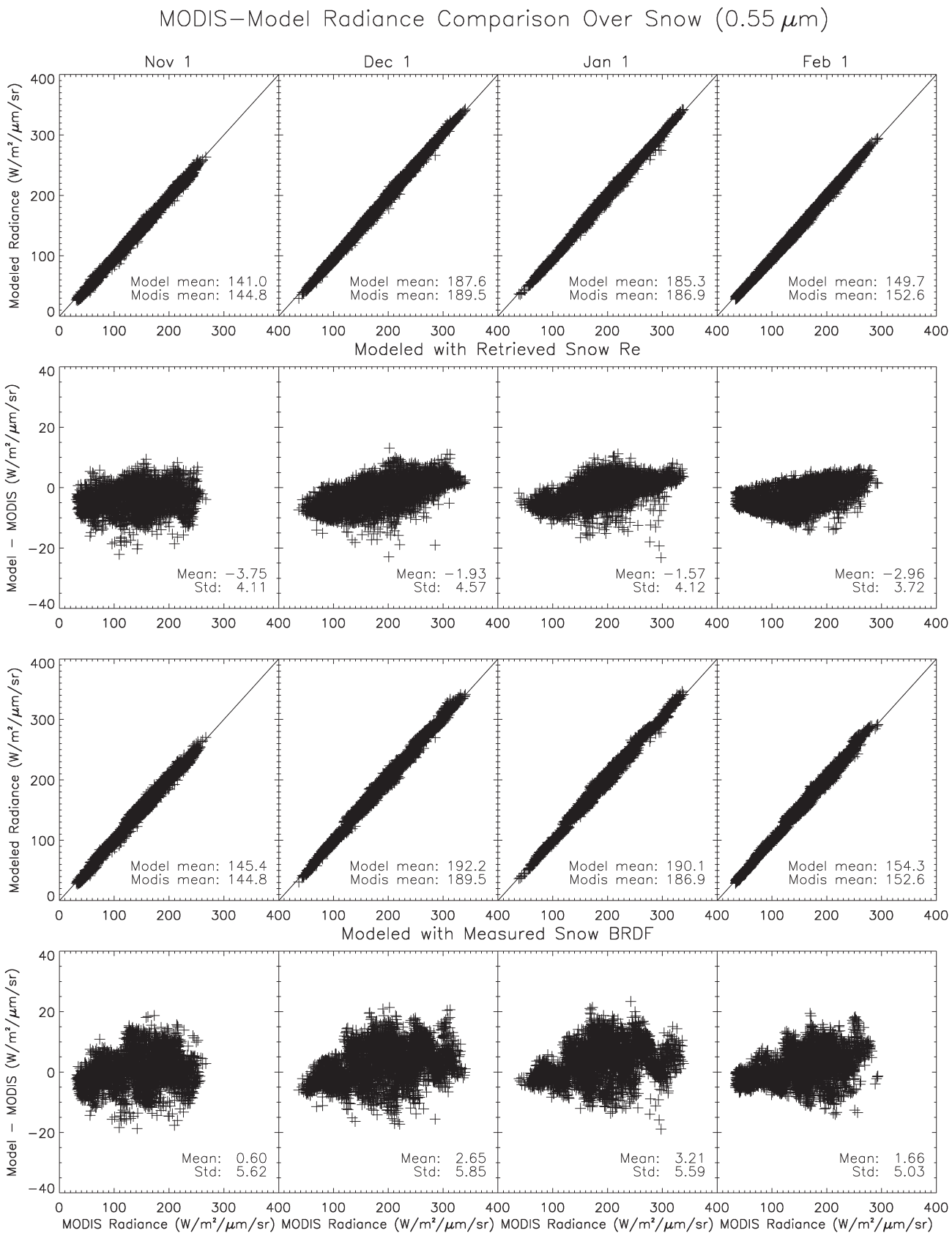

Fig. 15. Radiance comparison between model and MODIS measurements in channel 4 (0.55 μm). The four columns are for the four days and the five years of data for each date are combined together. The upper two rows show the modeled results using the retrieved RE as shown in Figs. 9 and 10, whereas the lower two rows show modeled results using the measured surface reflectance at Dome C. Only the clear CERES footprints with surface level higher than 2500 m above sea level are used to minimize the atmospheric effects.

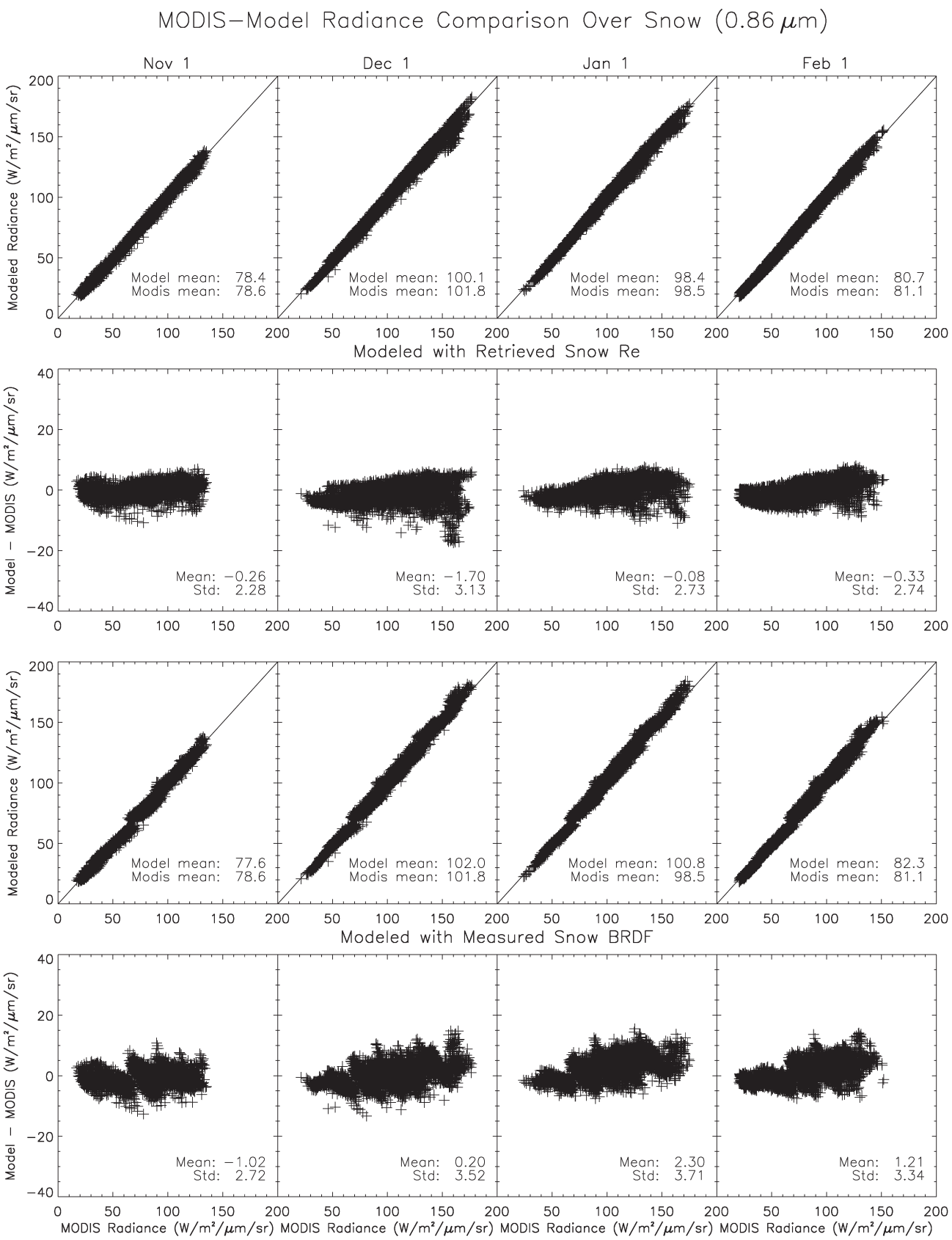

Fig. 16. Similar to Fig. 12, but for MODIS channel 2 (0.86 μm).

tens of percent smaller than those using ARF from Dome C (lower rows). However, for the 2.13 μm channel (Fig. 17), results from the simulation using only the local ARF from Dome C (lower rows) to represent the broad Antarctic plateau are not adequate. This is due to the high sensitivity of the 2.13 μm channel to snow grain size (see Fig. 6), which varies with time and location (Figs. 9–10). The 2.13 μm

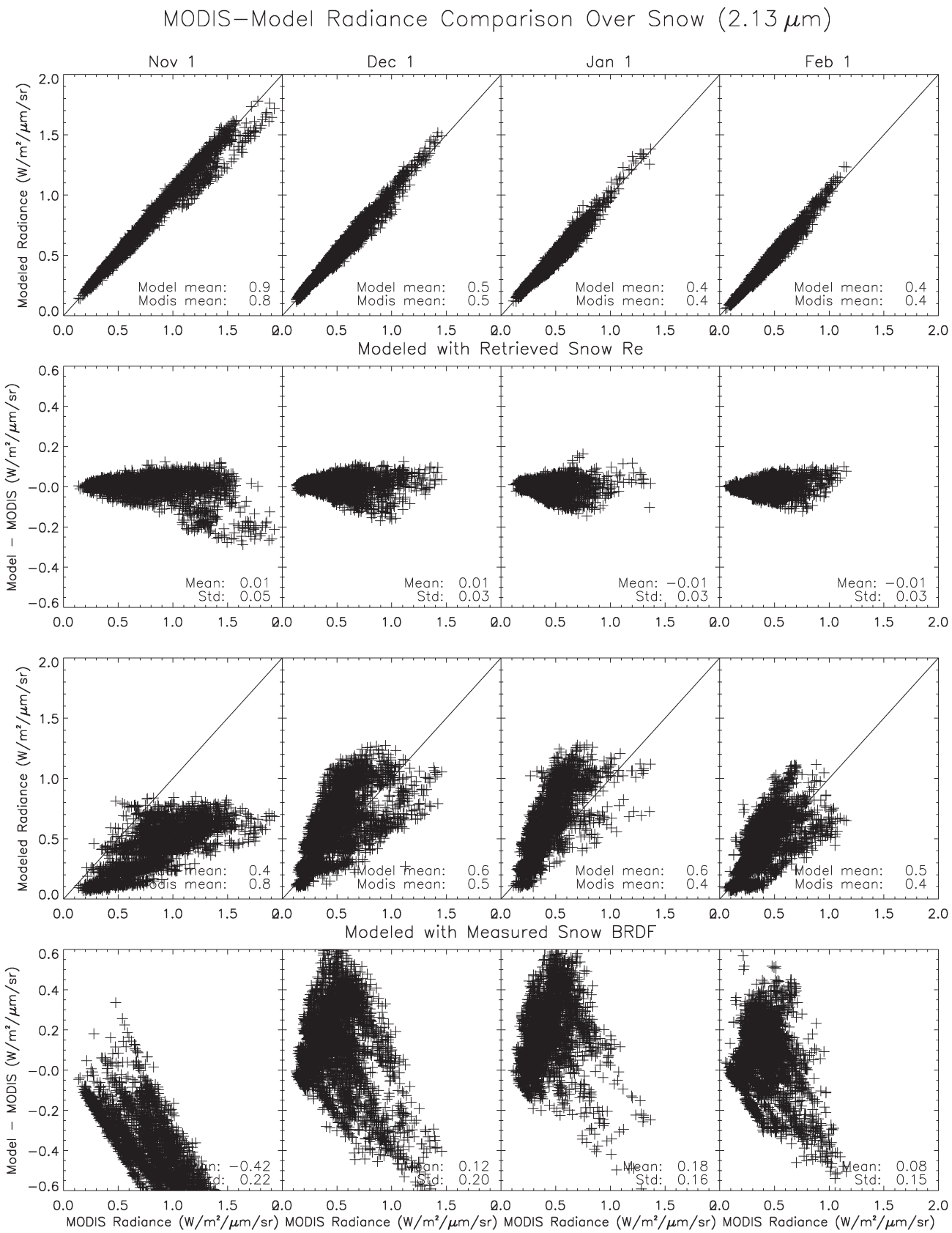

Fig. 17. Similar to Fig. 12, but for MODIS channel 7 (2.13 μm).

radiances calculated using retrieved grain sizes, which include information from MODIS at 1.64 μm, compare favorably with MODIS (upper rows of Fig. 17).

Fig. 18 extends the comparison of computed and observed radiances to the CERES broadband, where the absorption within the atmosphere is more significant than in the MODIS channels. The

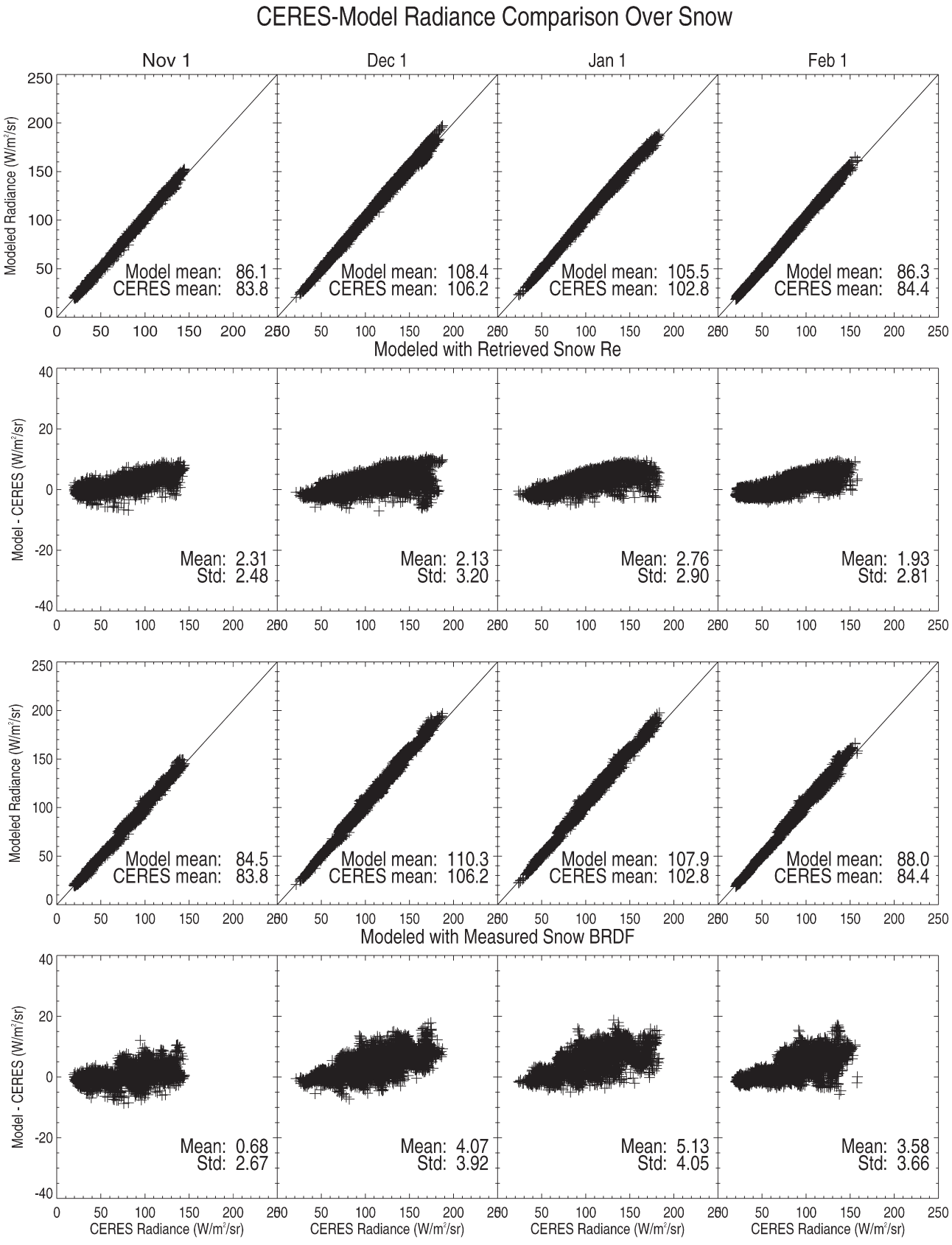

Fig. 18. Similar to Fig. 12, but for CERES broadband shortwave.

second set of calculations (the lower two rows) show a bit larger bias than the first set calculations, probably from the near infrared component of the shortwave radiation, where the grain size is important and the measured BRDF at one site is not representative. The reflected solar radiation over snow is, however, dominated by the shorter wavelengths. One half of the cumulative reflection to

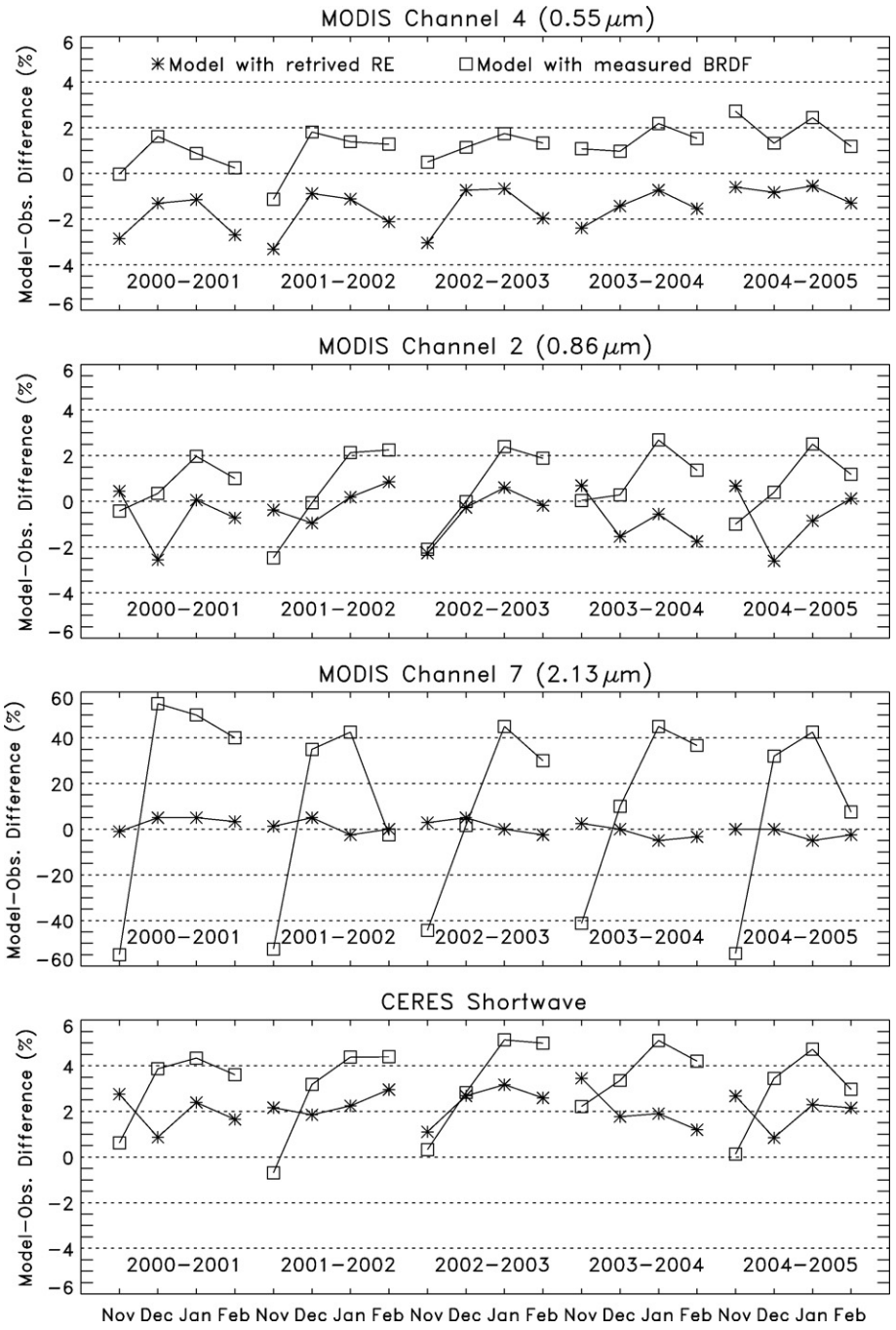

Fig. 19. The relative discrepancies for the modeled radiances shown in Figs. 15–18 in the three MODIS channels (the upper three panels) and the CERES shortwave (the lower panel). Results from four days each year from 2000 to 2005 as shown in Fig. 9 are presented.

TOA over the plateau occurs at wavelengths below 0.65 μm, for a solar zenith angle of 70°.

Fig. 19 shows the mean relative biases (model minus observation divided by observation) for the MODIS (0.55 μm, 0.86 μm, and 2.13 μm) and CERES channels shown above in Figs. 15–18. They are separated to year by year for the four days in each summer. The squares denote biases where the model uses measured surface ARF for input. The asterisks denote biases where the model uses grain sizes retrieved from MODIS (at 0.64 μm and 1.64 μm) within each respective CERES footprint. The biases for modeling with measured ARF (squares) in each of the lower panels (0.86 μm, 2.13 μm, and broadband) has a characteristic seasonal pattern (from November to February), but the range in bias is quite different from band to band; these seasonal patterns in bias are mostly due to the seasonal variation of the snow grain size. The measured ARF was at one location and in limited time period, and the calculations using this input (squares) therefore cannot represent the entire Antarctic plateau for each summer month in a 5-year span. Note the large seasonal variation for the grain size of the top layer in the upper panel of Fig. 11. As shown in Figs. 9 and 11, the snow grain size of the top layer is smallest in November each year and, therefore, the surface reflectance is largest and is likely larger than the measurements, which results in the bias to the low end in November each year for the modeled radiances with measured reflectance (squares) in the lower three panels of Fig. 19. The biases and their seasonal variations are largest for the 2.13 μm radiances, because of the high sensitivity of this channel to snow grain size. On

the other hand, we expect hardly any seasonal pattern of the model bias when using RE retrieved instantaneously for each footprint (asterisks), because the grain size variation is then already considered in model calculations.

The relative biases for calculations in the 0.55 μm channel (upper panel of Fig. 19) are almost counter intuitive. The seasonal variations of bias for the model using measured ARF (squares) are different from year to year and do not show the seasonal pattern as for the other three channels, but they are similar for the model biases using retrieved RE (asterisks). This occurs because the radiance at 0.55 μm is only marginally sensitive to RE, and the surface macroscale roughness hence emerges as the more important factor. The measured ARF includes the small surface roughness effect at Dome C. Surface roughness tends to reduce the forward reflection but enhance the backward reflection. Note that the satellite observations with large view angles in the forward scattering plane were excluded for model simulation here and the modeling using retrieved RE considered flat snow surface; this explains the consistent lower biases (i.e., less reflection) for plane-parallel modeling with retrieved RE (asterisks) than those using measured ARF (squares) in the upper panel of Fig. 19. The seasonal bias variation for modeling with measured ARF is also smallest in this channel.

The variations for the bias in the broadband are similar to those in the 0.86 μm band for radiances modeled with both approaches, indicating that the CERES broadband shortwave radiance has similar and moderate sensitivity to snow grain size as the MODIS 0.86 μm channel. The seasonal variation of snow grain size over the Antarctic plateau produces about 5% of variation in broadband shortwave reflectance. Note that the biases for CERES SW are mostly positive.

7. Conclusion

We calculated the single scattering snow optical properties for different particle shapes and degrees of microscopic scale surface roughness; and compared them. All of these optical properties (extinction, absorption, scattering asymmetry factor or phase function) vary with the effective particle radius (the snow grain size). When both grain size and total snow mass are held constant, the total optical extinction in the shortwave has almost no variation with change in particle shape, particle microscopic scale surface roughness, or wavelength. However, other optical properties (the single scattering albedo and asymmetry factor) vary strongly with snow particle shape and wavelength. Microscopic scale particle surface roughness mainly affects the scattering asymmetry factor and phase function; increasing roughness tends to smooth the scattering phase function.

The snow optical properties were implemented in a coupled atmosphere-snow radiative transfer model. The radiative transfer simulations were compared with quality surface and satellite measurements. The results showed that the radiation over snow is sensitive to the snow grain size and its vertical profile. When inhomogeneity of the particle size distribution is taken into account (e.g., by using a two-layer snow model), the measured spectral albedo can be successfully simulated, regardless of particle shape. But the modeled radiance distribution depends on the particle shape. The usual “equivalent spheres” assumption significantly overestimates forward reflected radiances, and underestimates backscattering radiances, around the principal plane. On average, the aggregate shape assumption has the best agreement with the measured radiances (mean discrepancy of less than 2% with the measured ARF).

Using the MODIS 1.64 μm and 0.64 μm data and the coupled atmosphere-snow radiative transfer model, we retrieved the snow grain size (aggregate assumption) over the Antarctic continent in clear conditions. The retrieved top layer grain size showed similar and large seasonal variation (e.g., increasing from November to December) in all years, but year-to-year variation was small. Retrieved snow particle grain sizes for the bottom layer were generally larger, and they had less seasonal variation, than those on the top. However, the retrieval algorithm is pertinent to the snow in the Antarctica. For snow in other regions, where size is large and the atmospheric effect is larger, a retrieval algorithm would require more inputs than the two MODIS channels used here.

The retrieved snow grain sizes (based on MODIS 1.64 μm and 0.64 μm data) were used to model the spectral radiances of three other MODIS channels and the broadband shortwave radiances of CERES. Except for the MODIS 2.13 μm channel, the mean relative model-observation differences are generally a few percent. These modeled narrow-band and broadband radiances with a 2-layer snow retrieval for input were also compared with those modeled using the measured surface reflectance at Dome C for input. The results indicate that the measured surface reflectance covering the MODIS 0.55 μm channel at Dome C can be applied to the snow over the entire Antarctic plateau, whereas those in the near infrared 2.13 μm channel cannot be used to represent the snow in other locations or at other times, because of the high sensitivity of the near infrared to the snow grain size (which has spatial and temporal variation). The broadband shortwave radiance is moderately sensitive to the snow grain size, comparable to the MODIS 0.86 μm channel. The broadband snow surface albedo over the Antarctic plateau is not a constant, but varies around 5% in a year; this is mostly due to a seasonal variation in snow grain size. CERES broadband radiances simulated with retrieved grains sizes are about 2% larger than those observed.

Significant discrepancies between calculations and observations show that satellite observations with large view zenith angles around the principal plane should be avoided for the retrieval of snow properties. The results also provide guidance to improve the accuracy of a calculation for the radiative energy budget over snow. A two-layer snow model with retrieved snow grain sizes from the coincident MODIS measurements will be used in a future CERES algorithm.

Acknowledgements

We thank Dr. Stephen Warren and Dr. Steve Hudson at University of Washington for the field measurement data. The satellite data were processed at the NASA Langley Research Center Atmospheric Science Data Center. Dr. Victor Sothcott helped for the data inversion. Dr. Grant Matthews provided the Rev1 calibration for the CERES data. We also thank the very useful comments from the three reviewers.

References

Aoki, T., Aoki, T., Fukabori, M., Hachikubo, A., Tachibana, Y., & Nishio, F. (2000). Effects of snow physical parameters on spectral albedo and bidirectional reflectance of snow surface. *J. Geophys. Res.*, *105*(D8), 10,219–10,236.

Bloom, S., da Silva, A., Dee, D., Bosilovich, M., Chern, J. D., Pawson, S., et al. (2005). Documentation and Validation of the Goddard Earth Observing System (GEOS) Data Assimilation System — Version 4. *Technical Report Series on Global Modeling and Data Assimilation*, *vol. 104606* (pp. 26).

Chamberlin, R. A. (2001). South Pole submillimeter sky opacity and correlations with radiosonde observations. *Journal of Geophysical Research*, *106*, 20101–20113.

Charlock, T. P., Rose, F. G., Rutan, D. A., Jin, Z., & Kato, S. (2006). The global surface and atmosphere radiation gadget: An assessment of accuracy with 5 years of calculations and observations. *Proceedings of 12th Conference on Atmospheric Radiation (AMS), 10–14 July, 2006*. Wisconsin: Madison.

Cox, C., & Munk, W. (1954). Measurement of the roughness of the sea surface from photographs of the sun glitter. *Journal of the Optical Society of America*, *44*, 838–850.

Gay, M., Fily, M., Genthon, C., Frezzotti, M., Oerter, H., & Winther, J. G. (2002). Snow grain-size measurements in Antarctica. *Journal of Glaciology*, *48*(163), 527–535.

Grenfell, T. C., Warren, S. G., & Mullen, P. C. (1994). Reflection of solar radiation by the Antarctic snow surface at ultraviolet, visible, and near-infrared wavelengths. *Journal of Geophysical Research*, *99*, 18,669–18,684.

Henyey, L. G., & Greenstein, J. L. (1941). Diffuse radiation in the galaxy. *Astrophysical Journal*, *93*, 70–83.

Hudson, S. R., Warren, S. G., Brandt, R. E., Grenfell, T. C., & Six, D. (2006). Spectral bidirectional reflectance of Antarctic snow: Measurements and parameterization. *Journal of Geophysical Research*, *111*, D18106. doi:10.1029/2006JD007290

Jin, Z., Charlock, T. P., Rutledge, K., Stamnes, K., & Wang, Y. (2006). An analytical solution of radiative transfer in the coupled atmosphere-ocean system with rough surface. *Applied Optics*, *45*, 7443–7455.

Kaufman, Y. J., Tanre, D., Gordon, H. R., Nakajima, T., Lenoble, J., Frouin, R., et al. (1997). Passive remote sensing of tropospheric aerosol and atmospheric correction for the aerosol effect. *Journal of Geophysical Research*, *102*, 16,815–16,830.

Kokhanovsky, A. A., & Zege, E. P. (2004). Scattering optics of snow. *Applied Optics*, *43*, 1589–1602.

Li, S., & Zhou, X. (2004). Modeling and measuring the spectral bidirectional reflectance factor of snow-covered sea ice: An intercomparison study. *Hydrology Processes*, *18*, 3559–3581.

McClatchey, R. A., Fenn, R. W., Selby, J. E. A., Volz, F. E., & Garing, J. S. (1972). Optical properties of the atmosphere. *AFCRL report AFCRL-72-0497*. Bedford, MA: Air Force Cambridge Laboratories.

Minnis, P., Young, D. F., Sun-Mack, S., Heck, P. W., Doelling, D. R., & Trepte, Q. (2003). CERES cloud property retrievals from imagers on TRMM, terra, and aqua. *Proc. SPIE 10th International Symposium on Remote Sensing: Conference on Remote Sensing of Clouds and the Atmosphere*, *VII* (pp. 37–48).Spain: Barcelona September 8–12.

Mishchenko, M. I., Dlugach, J. M., Yanovitskij, E. G., & Zakharova, N. T. (1999). Bidirectional reflectance of flat, optically thick particulate layers: an efficient radiative transfer solution and applications to snow and soil surfaces. *JQSRT*, *vol. 63* (pp. 409–432).

Nolin, A. W., & Dozier, J. (2000). A hyperspectral method for remotely sensing the grain size of snow. *Remote Sensing of Environment*, *74*(2), 207–216.

Painter, T. H., & Dozier, J. (2004). Measurements of the hemispherical–directional reflectance of snow at fine spectral and angular resolution. *Journal of Geophysical Research*, *109*(D18), D18115. doi:10.1029/2003JD004458

Priestley, K. J., Kopia, L. P., Lee, R. B., Mahan, J. R., Haeffelin, M. P., Smith, G. L., et al. (1997). Use of first-principle numerical models to enhance the understanding of the CERES point spread function. In Hiroyuki Fujisada (Ed.), *Sensors, Systems, and Next-Generation SatellitesProceeding SPIE*, *vol. 3221* (pp. 191–200).

Warren, S. G. (1984). Optical constants of ice from the ultraviolet to the microwave. *Applied Optics*, *23*, 1206–1225.

Warren, S. G., Brandt, R. E., & O'Rawe Hinton, P. (1998). Effect of surface roughness on bidirectional reflectance of Antarctic snow. *Journal of Geophysical Research*, *103*, 25,789–25,807.

Wielicki, B. A., Barkstrom, B. R., Harrison, E. F., Lee, R. B., Smith, G. L., & Cooper, J. E. (1996). Clouds and the Earth s Radiant Energy System (CERES): An Earth observing system experiment. *Bullutin of the American Meteorological Society*, *77*, 853–868.

Wiscombe, W. J., & Warren, S. G. (1980). A model for the spectral albedo of snow. I: Pure snow. *Journal of the Atmospheric Science*, *37*, 2712–2733.

Xie, Y., Yang, P., Gao, B. C., Kattawar, G. W., & Mishchenko, M. I. (2006). Effect of ice crystal shape and effective size on snow bidirectional reflectance. *Journal of Quantitative Spectroscopy and Radiative Transfer*, *100*, 457–469.

Yang, P., & Liou, K. N. (1998). Single-scattering properties of complex ice crystals in terrestrial atmosphere. *Contributions Atmospheric Physics*, *71*, 223–248.

Yang, P., & Liou, K. N. (1996). Geometric-Optics-integral-equation method for light scattering by nonspherical ice crystals. *Applied Optics*, *35*, 6568–6584.